Supporting Information

A Novel Strategy to Construct Janus Metallamacrocycles with both Ru-arene Face and Imidazolium Face

Ji Li,[a‡] Peipei Zhang,[a‡] Yan Xu,[d] Zhi Su,[a] Yong Qian,[*a] Shunli Li,[a] Tao Yu,[*c] Peter J. Sadler,[*b] Hong-Ke Liu[*a]

a. Jiangsu Collaborative Innovation Center of Biomedical Functional Materials, College of Chemistry and Materials Science, Nanjing Normal University, Nanjing, 210046, China. E-mail: liuhongke@njnu.edu.cn; yongqian@njnu.edu.cn

b. Department of Chemistry, University of Warwick, Gibbet Hill Road, Coventry, CV4 7AL, UK E-mail: P.J.Sadler@warwick.ac.uk

c. Department of Chemistry, Tennessee Tech University,1 William L Jones Dr, Cookeville, TN 38505 USA. Email: tyu@tntech.edu

d. College of Chemistry and Chemical Engineering, Nanjing University of Technology, Technology, Nanjing, 210009, P. R. China.

Contents

Table S1. Crystallographic data of complexes **1**-**2**.

Table S2. Selected bond lengths [Å] and angles (°) for **1** and **2**.

Table S3. H-bonds observed between the RuL_2CH_2 metallamacrocycle and trapped Cl^- anion.

Table S4. The coordination bond length and other geometry profiles, Ru-Ru and N1-N1 distance in the complexes.

Table S5. IC_{50} values of RuL_2CH_2 complexes towards different cell lines *in vitro.*

Scheme S1. Schematic representation of the possible pathways for the formation of RuL_2CH_2 complexes.

Figure S1. Chemical structure and NMR numbering schemes of Ru(II)-arene metallamacrocycles complexes (**1**-**3**).

Figure S2. Photograph of the crystals and crystal size of **1a** that were observed under a microscope.

Figure S3. Crystal structure of the "bowl-like" mononuclear RuL_2CH_2 metallamacrocycle **1b**.

Figure S4. Crystal structure of the "bowl-like" mononuclear RuL_2 metallamacrocycle **1c**.

Figure S5. ESI-MS analysis for the reaction of $[RuCl_2(\eta^6\text{-bip})]_2$ and p-bitmb in CH_2Cl_2.

Figure S6. Pictures of reaction vials for **1a** obtained at different reaction temperatures.

Figure S7. Changes in the absorption spectra of **1a** upon addition of various anions.

Figure S8. Changes in the absorption spectra of **2** upon addition of various anions.

Figure S9. Changes in the absorption spectra of **3** upon addition of various anions.

Figure S10. The ESI-MS spectra of **1c**.

Figure S11. The ESI-MS spectra of **2**.

Figure S12. The ESI-MS spectra of **3**.

Table S1. Crystallographic data of complexes **1-2**

Compound	**1a**	**1b**	**1c**	**2**
Formula	$RuC_{47}H_{82}N_8O_{11}Cl_4$	$RuC_{51}H_{68}N_8Cl_{12}$	$RuC_{50}H_{65}N_8OCl_{9.75}I_{0.25}$	$RuC_{53}H_{65.5}N_8O_{0.75}Cl_{12}$
Weight	1178.07	1319.6	1272.53	1353.10
Crystal system	Monoclinic	Monoclinic	Monoclinic	Monoclinic
Space group	$P2_1/c$	$P2_1/c$	$P2_1/c$	$P2_1/c$
Wavelength(Å)	0.71069	0.71073	0.71073	0.71073
Collection T (K)	293(2)	100(2)	100(2)	100(2)
a(Å)	12.568(5)	21.086 (3)	12.694(5)	12.964 (5)
b(Å)	31.904(5)	23.518 (4)	31.347(12)	30.036 (11)
c(Å)	14.478(5)	14.273 (3)	14.646(6)	15.807 (6)
α(°)	90.000	90.000	90.000	90.000
β(°)	96.956(5)	104.275 (4)	98.607(5)	106.065 (4)
γ(°)	90.000	90.000	90.000	90.000
V (A $^{\circ 3}$)	5763(3)	6859 (2)	5762(4)	5915 (4)
Z	4	4	4	4
D_{calc} (mg m^{-3})	1.358	1.278	1.467	1.520
F (000)	2480	2712	2608	2774
θ range /º	1.8 to 25	2.3 to 25.50	1.5 to 25	1.5 to 21.9
Limiting indices	-11 ≤ h ≤ 14, -37 ≤ k ≤ 32, -17 ≤ l ≤ 16	-25 ≤ h ≤ 25, -28 ≤ k ≤ 28, -17 ≤ l ≤ 16	-14 ≤ h ≤ 15, -37 ≤ k ≤ 37, -17 ≤ l ≤ 15	-13 ≤ h ≤ 13, -30 ≤ k ≤ 31, -16 ≤ l ≤ 16
Reflections collected/ unique	5778/10139	11465/12686	8916/10036	5431/7081
R(int)	0.057	0.023	0.057	0.101
Completeness to theta = 25.00	99.0%	99.2%	98.6%	99.0%
Refinement method	Full-matrix least-squares on F^2	Full-matrix least-squares on F^2	Full-matrix least-squares on F^2	Full-matrix least-squares on F^2
Data / restraints / parameters	10139 / 27 / 554	12689/0/658	10036/8/641	7081/42/704
Goodness-of-fit on F^2	0.903	1.042	1.152	1.197

Final R indices [I>2sigma(I)]	R_1 =0.0454 wR_2 =0.1231	R_1 =0.0462 wR_2 =0.1362	R_1 =0.1138 wR_2 =0.2743	R_1 =0.0765 wR_2 =0.1759

[a]$R_1 = \Sigma||F_o| - |F_c||/\Sigma|F_o|$.[b]$wR_2 = |\Sigma w(|F_o|^2 - |F_c|^2)/\Sigma|w(F_o)^2|^{1/2}$, where $w = 1/[\sigma^2(F_o^2) + (aP)^2 + bP]$. $P = (F_o^2 + 2F_c^2)/3$.

Table S2. Selected bond lengths [Å] and angles (°) for **1** and **2**

1a			
Ru1-N1	2.113(3)	Ru1-C40	2.208(5)
Ru1-N8	2.105(3)	Ru1-C41	2.159(4)
Ru1-C6	2.159(4)	Ru1-C42	2.175(5)
Ru1-C39	2.159(5)	Ru1-C43	2.193(6)
Ru1-Cl1	2.4198(15)	N4-C1	1.444(5)
C1-N5	1.455(5)	Ru1---C1	7.3
J1---J2	5.2		
N8-Ru1-N1	86.81(10)	N1-Ru1-Cl1	86.80(8)
N8-Ru1-Cl1	87.36(8)	N4-C1-N5	112.0(3)
1b			
Ru1-N1	2.119(3)	Ru1-C40	2.211(3)
Ru1-N8	2.098(2)	Ru1-C41	2.168(3)
Ru1-C6	2.181(3)	Ru1-C42	2.198(3)
Ru1-C39	2.165(3)	Ru1-C43	2.210(3)
Ru1-Cl1	2.4212(9)	N4-C1	1.453(4)
C1-N5	1.461(4)	Ru1---C1	6.7
J1---J2	5.4		
N8-Ru1-N1	85.54(10)	N1-Ru1-Cl1	87.88(7)
N8-Ru1-Cl1	87.51(7)	N4-C1-N5	111.2(2)
1c			
Ru1-N1	2.122(9)	Ru1-C40	2.202(10)
Ru1-N8	2.114(8)	Ru1-C41	2.181(10)
Ru1-C6	2.172(10)	Ru1-C42	2.184(13)
Ru1-C39	2.177(9)	Ru1-C43	2.191 (11)
Ru1-Cl1	2.422(3)	N4-C1	1.443(12)
C1-N5	1.473(11)	Ru1---C1	7.4
J1---J2	5.1		
N8-Ru1-N1	88.3(3)	N1-Ru1-Cl1	86.9(2)
N8-Ru1-Cl1	87.5(2)	N4-C1-N5	111.4(7)
2			
Ru1-N1	2.107(9)	Ru1-C40	2.180(10)
Ru1-N8	2.108(8)	Ru1-C41	2.183(9)
Ru1-C6	2.184(9)	Ru1-C42	2.194(10)

Ru1-C39	2.182(10)	Ru1-C43	2.175(9)
Ru1-Cl1	2.418(3)	N4-C1	1.456(12)
C1-N5	1.447(12)	Ru1---C1	6.8
J1---J2	5.3		
N8-Ru1-N1	86.3(3)	N1-Ru1-Cl1	87.8(2)
N8-Ru1-Cl1	87.6(2)	N4-C1-N5	112.3(7)

Table S3. H-bonds observed between the RuL_2CH_2 metallamacrocycle and trapped Cl^- anion.

Complex **1a**			
D—H···A	Distance(D···A)	D-H-A angle	（D-H-A）
C6—H6···Cl2	3.550	C6-H6-Cl2	141.64
C7—H7···Cl2	3.675	C7-H7-Cl2	170.33
C8—H8···Cl2	3.391	C8-H8-Cl2	150.32
C9—H9···Cl2	3.324	C9-H9-Cl2	154.08
C10—H10···Cl2	3.739	C10-H10-Cl2	166.58
Complex **1b**			
D—H···A	Distance(D···A)	D-H-A angle	（D-H-A）
C6—H6···Cl2	3.440	C6-H6-Cl2	150.97
C7—H7···Cl2	3.608	C7-H7-Cl2	163.68
C8—H8···Cl2	3.336	C8-H8-Cl2	136.78
C9—H9···Cl2	3.323	C9-H9-Cl2	147.34
C10—H10···Cl2	3.703	C10-H10-Cl2	171.88
C11—H11···Cl2	3.811	C11-H11-Cl2	149.78
Complex **1c**			
D—H···A	Distance(D···A)	D-H-A angle	（D-H-A）
C6—H6···Cl2	3.531	C6-H6-Cl2	137.67
C7—H7···Cl2	3.596	C7-H7-Cl2	170.76
C8—H8···Cl2	3.473	C8-H8-Cl2	147.47
C9—H9···Cl2	3.377	C9-H9-Cl2	153.54
C10—H10···Cl2	3.916	C10-H10-Cl2	166.94
Complex **2**			
D—H···A	Distance(D···A)	D-H-A angle	（D-H-A）
C6—H6···Cl2	3.405	C6-H6-Cl2	132.71
C7—H7···Cl2	3.624	C7-H7-Cl2	169.06
C8—H8···Cl2	3.341	C8-H8-Cl2	151.02
C9—H9···Cl2	3.369	C9-H9-Cl2	150.42
C10—H10···Cl2	3.621	C10-H10-Cl2	163.45

Table S4. The coordination bond length and other geometry profiles, Ru-Ru and N1-N1 distance in the complexes in the unit of Å

	Ru-Cl	Ru-C	Ru-N	N1-N1	Ru-Ru
$Ru(cym)L_2CH_2$ (1)	2.48 (2.42)	2.28 (2.21)	2.10, 2.10 (2.09, 2.09)	2.47 (2.39)	--
$Ru(cym)L_2$ (4)	2.51	2.32	2.10, 2.10	7.37	--
$Ru_2(cym)_2L_2$ (5)	2.49 / 2.49	2.26 / 2.28	2.094, 2.101 /2.095, 2.101	--	8.15
$Ru_2(cym)_2L_3$ (6)	2.50 / 2.45	2.30 /2.32	2.11, 2.08 /2.11, 2.10	--	7.76

[a] The distances in the parentheses were from the corresponding crystal structure

Table S5. IC_{50} values of RuL_2CH_2 complexes towards different cell lines *in vitro*. [a]IC_{50} values are drug concentrations necessary for 50% inhibition of cell viability. Data are presented as means ± standard deviations obtained in at least three independent experiments

Complex	IC_{50} (μM)[a]		
	A549	Hela	L02
1	71.7±3.8	82.5±1.6	>200
2	>200	90.4±8.8	180.0±10.1
cisplatin	10.1±0.74	15.8±0.9	4.44±0.25

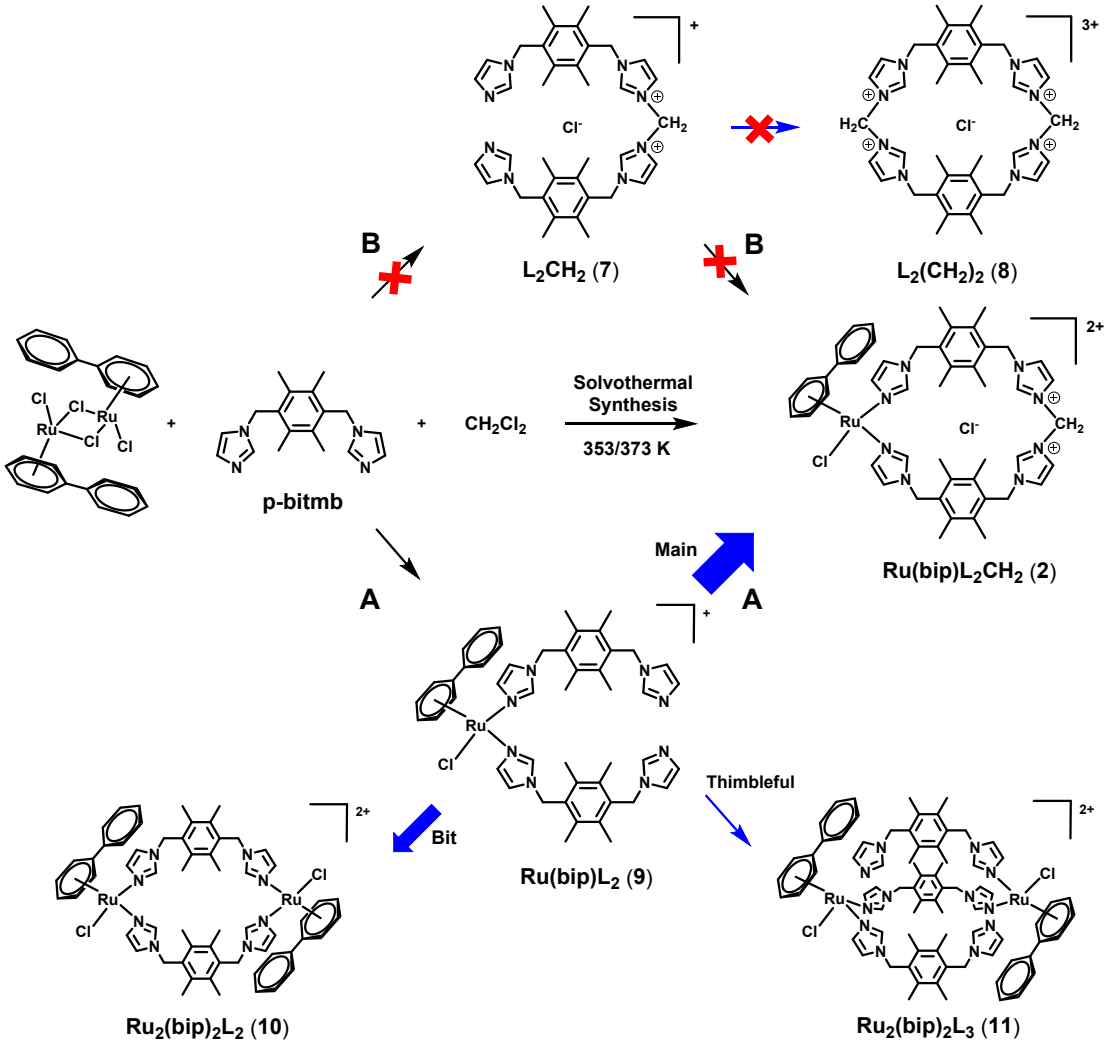

Scheme S1 Schematic representation of the possible pathways for the formation of RuL_2CH_2 complexes. The structures of the complexes (**2** and **9-11**) were successfully calculated and obtained by ESI-MS. These results indicated that the complex **2** was constructed via Pathway A.

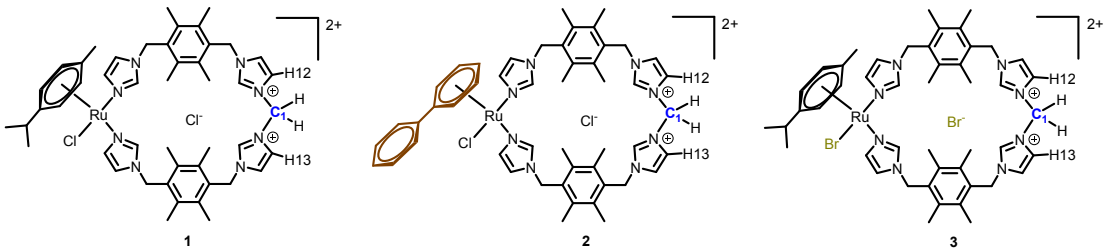

Figure S1. Chemical structure and NMR numbering schemes of Ru(II)-arene metallocyclic complexes (**1**-**3**)

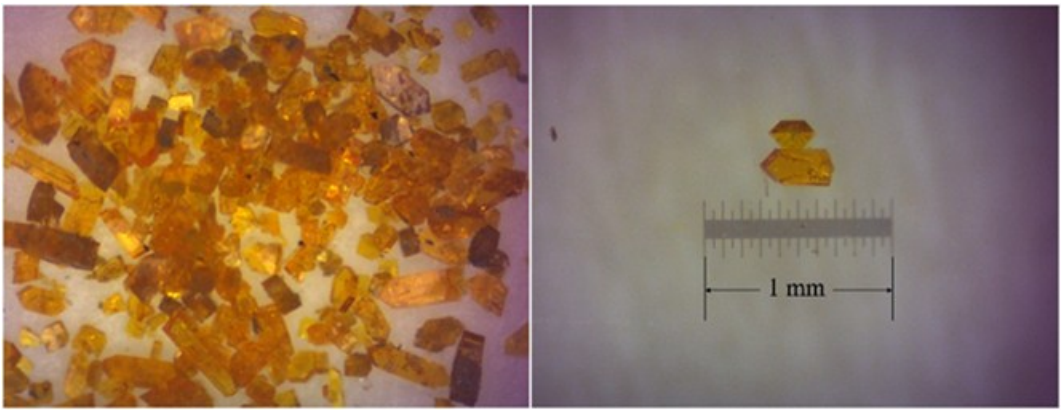

Figure S2. Photograph of the crystals and crystal size of **1a** that were observed under a microscope.

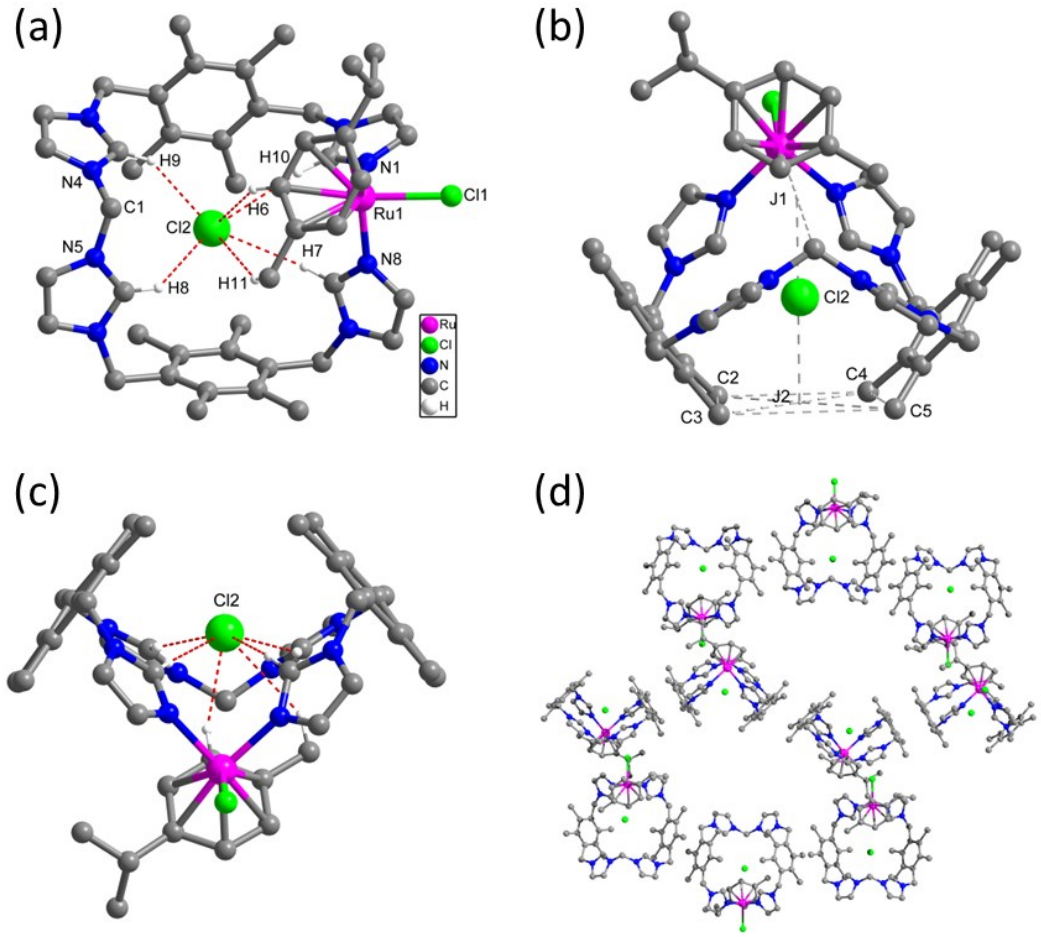

Figure S3. (a) Crystal structure of the "bowl-like" mononuclear RuL_2CH_2 metallamacrocycle **1b** (CH_2Cl_2, 373 K) with a Cl anion trapped inside of the cavity, forming 6 H-bonds. (b) The size of the "bowl-like" cavity was defined by the deep length (J1---J2, 5.4 Å) and diameter (Ru---C1, 6.7 Å). (c) Side view to show the trapped chloride anion inside the "bowl-like" structure. (d) The paking mode of **1b**.

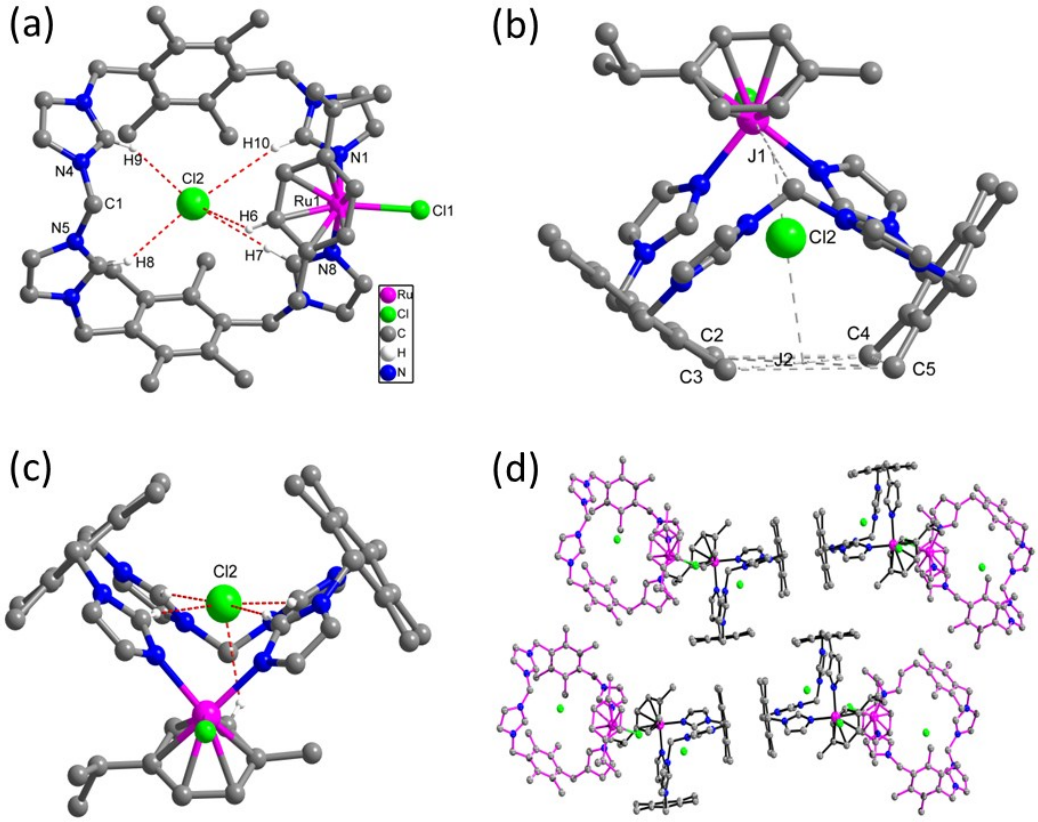

Figure S4. (a) Crystal structure of the "bowl-like" mononuclear RuL_2 metallamacrocycle **1c** ($RuI_2(\eta^6$-*p*-cymene), CH_2Cl_2, 353 K) with a Cl anion trapped inside of the cavity, forming 5 H-bonds. (b) The size of the "bowl-like" structure was defined by the deep length (J1---J2, 5.1 Å) and diameter (Ru---C1, 7.4 Å). (c) Side view to show the trapped chloride anion inside the "bowl-like" structure. (d) The packing mode of **1c**.

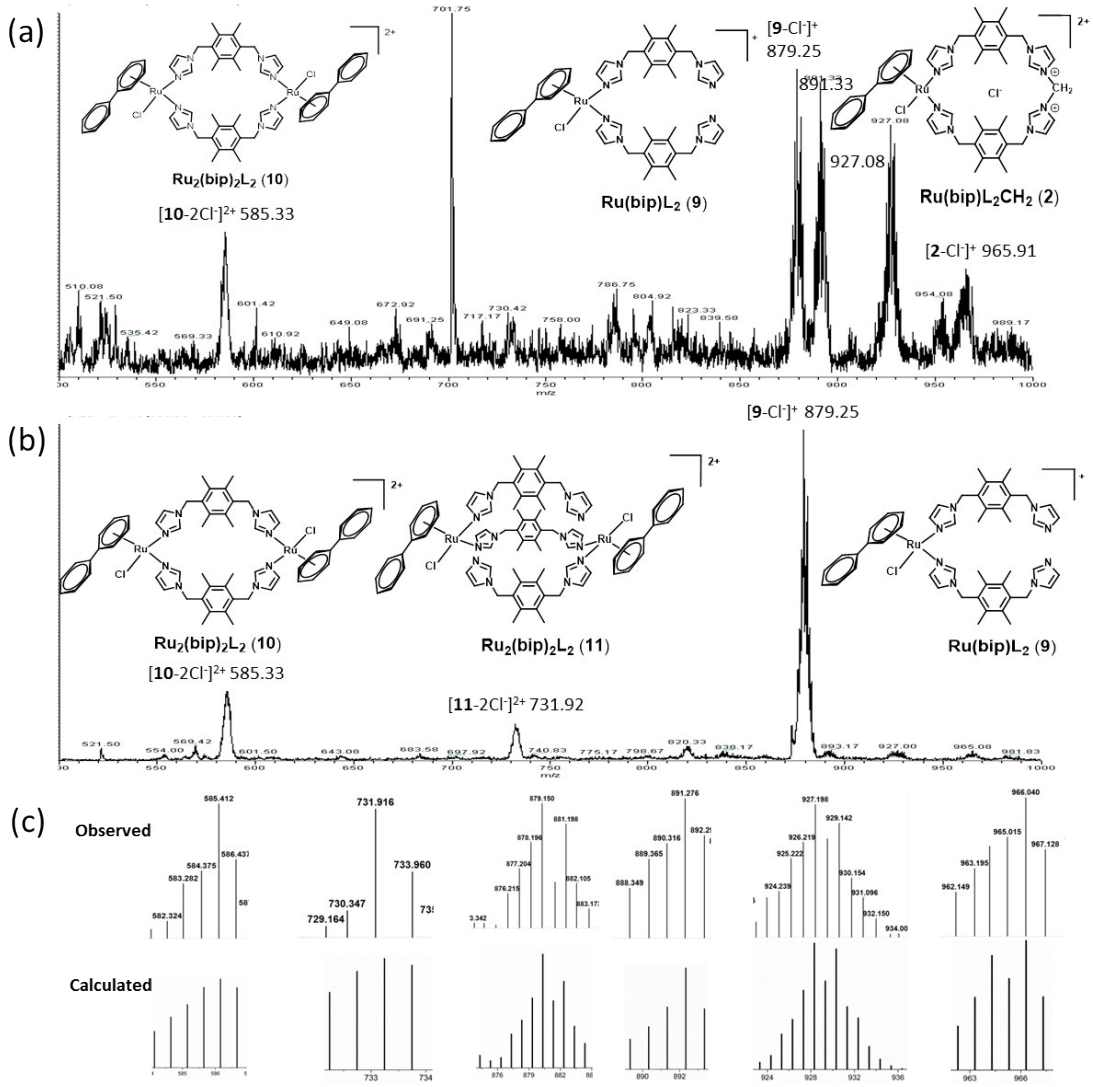

Figure S5. The ESI-MS spectra of the solvothermal reaction solution of $[RuCl_2(\eta^6\text{-bip})]_2$ and p-bitmb in CH_2Cl_2 heated at 373 K after 6 h in the resulted reaction solid (a) and solution (b); (c) calculated and observed ESI-MS spectra of complexes with isotopic distribution.

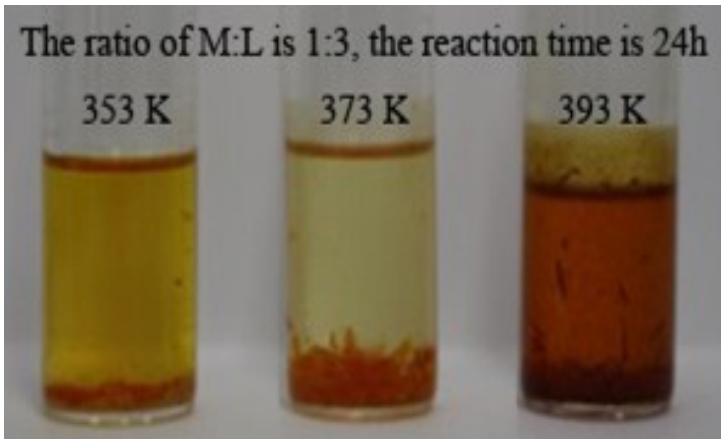

Figure S6. Pictures of reaction vials for 1a obtained at different reaction temperatures and highest yield was observed at 373 K.

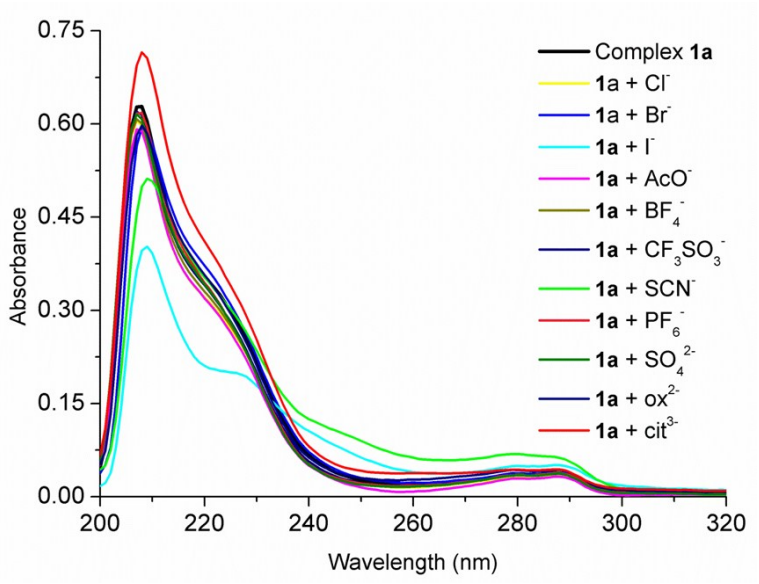

Figure S7. Changes in the absorption spectra of **1a** in methanol upon addition of incremental amounts of aqueous solutions of various anions (Cl^- = sodium chloride, Br^- = potassium bromide, I^- = lithium iodide, AcO^- = ammonium acetate, BF_4^- = Sodium Tetrafluoroborate, $CF_3SO_3^-$ = Lithium triflate, SCN^- = sodium sulfocyanate, PF_6^- = ammonium hexafluorophosphate, SO_4^{2-} = ammonium sulfate, ox^{2-} = ammonium oxalate, cit^{3-} = sodium citrate).

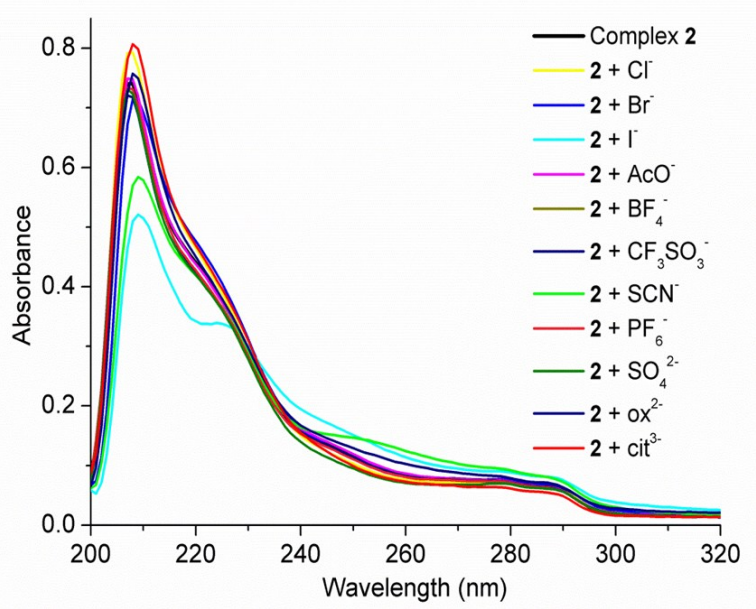

Figure S8. Changes in the absorption spectra of **2** in methanol upon addition of incremental amounts of aqueous solutions of various anions (Cl^- = sodium chloride, Br^- = potassium bromide, I^- = lithium iodide, AcO^- = ammonium acetate, BF_4^- = Sodium Tetrafluoroborate, $CF_3SO_3^-$ = Lithium triflate, SCN^- = sodium sulfocyanate, PF_6^- = ammonium hexafluorophosphate, SO_4^{2-} = ammonium sulfate, ox^{2-} = ammonium oxalate, cit^{3-} = sodium citrate).

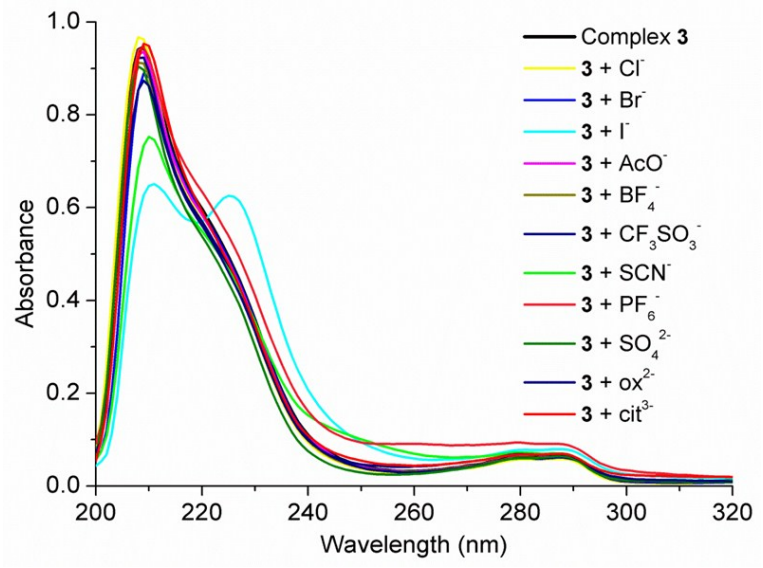

Figure S9. Changes in the absorption spectra of **3** in methanol upon addition of incremental amounts of aqueous solutions of various anions (Cl^- = sodium chloride, Br^- = potassium bromide, I^- = lithium iodide, AcO^- = ammonium acetate, BF_4^- = Sodium Tetrafluoroborate, $CF_3SO_3^-$ = lithium triflate, SCN^- = sodium sulfocyanate, PF_6^- = ammonium hexafluorophosphate, SO_4^{2-} = ammonium sulfate, ox^{2-} = ammonium oxalate, cit^{3-} = sodium citrate).

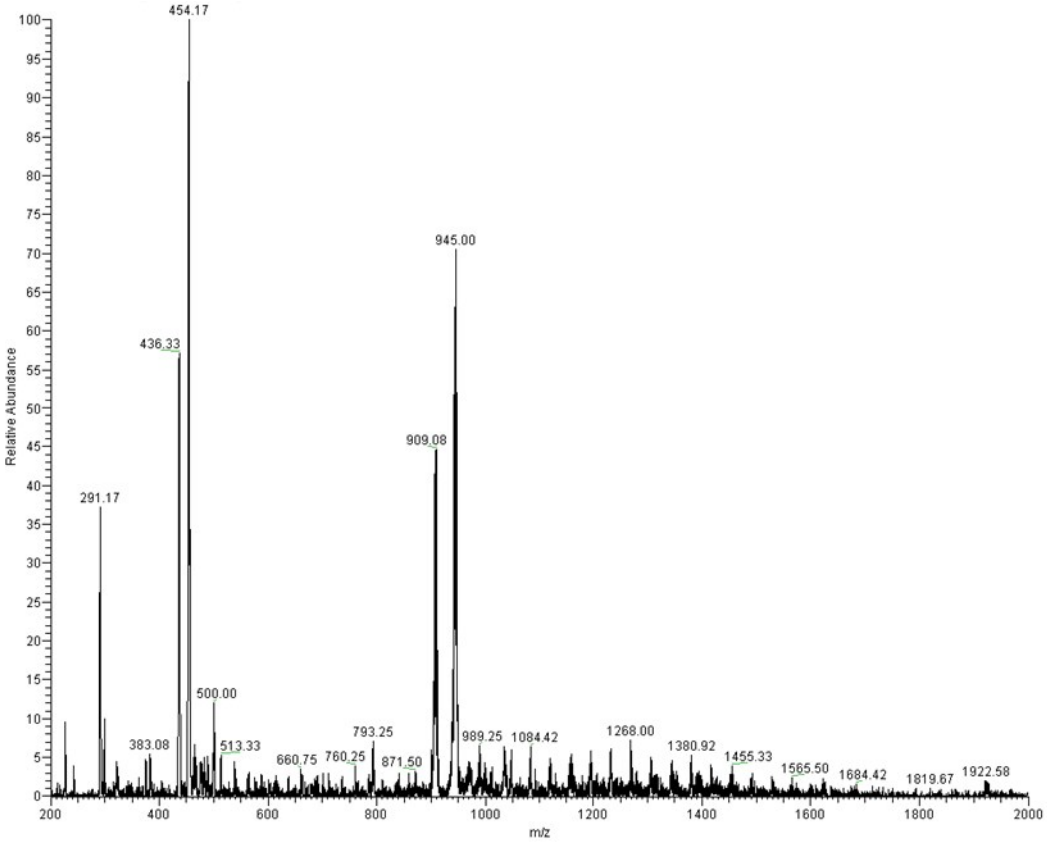

Figure S10. The ESI-MS spectra of **1c**

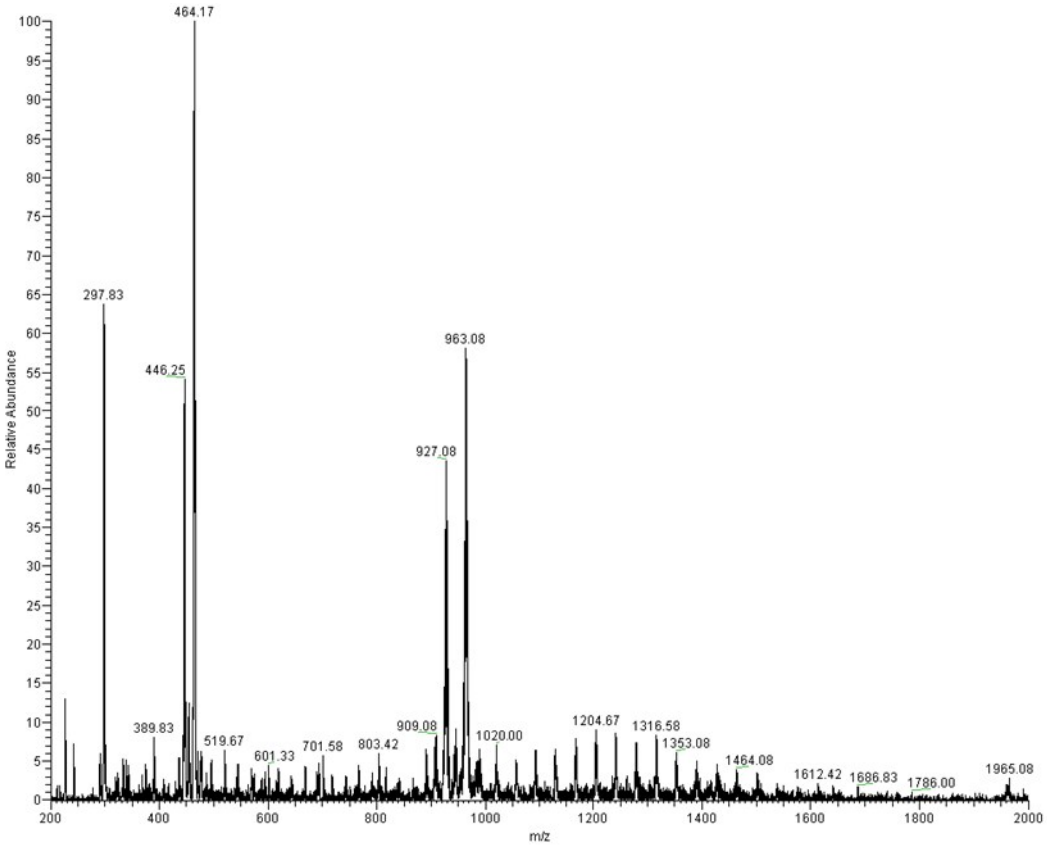

Figure S11. The ESI-MS spectra of **2**

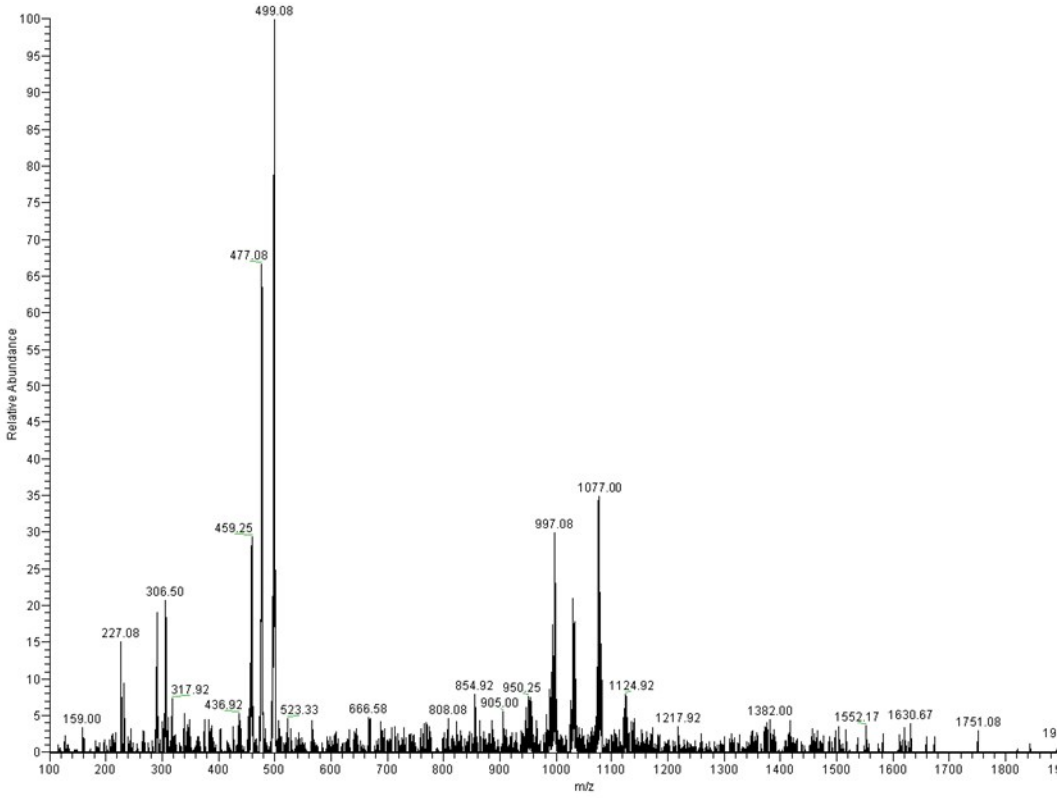

Figure S12. The ESI-MS spectra of **3**